Numerical Heat Transfer, Part B, 55: 503–522, 2009
Copyright © Taylor & Francis Group, LLC
ISSN: 1040-7790 print/1521-0626 online
DOI: 10.1080/10407780902864755

Taylor & Francis
Taylor & Francis Group

Downloaded by [China Science & Technology University] at 02:33 26 February 2014

NUMERICAL STUDY OF AN ELECTRO-OSMOTICALLY DRIVEN MICROCHANNEL FLOW WITH JOULE HEATING EFFECT

Tony W. H. Sheu and S. H. Kuo
Department of Engineering Science and Ocean Engineering, National Taiwan University, Taipei, Taiwan, Republic of China

A convection-diffusion reaction scheme is applied to solve the transient transport equations for the prediction of steady electro-osmotic microchannel flow behavior. The governing equations for the total electric field include the Laplace equation for the effective electrical potential and the Poisson-Boltzmann equation for the electrical potential established in the electric double layer. The transport equations governing the hydrodynamic field variables comprise mass conservation equation for the electrolyte and equations of motion for the incompressible charged fluid flow subject to an electro-osmotic body force. The main aim of the study is to elucidate the effect of Joule heating, which can affect the electrohydrodynamic behavior. Investigation into the region near the negatively charged channel wall is made through the simulated velocity boundary layer, diffuse layer, and electric double layer.

1. INTRODUCTION

Investigation into microfluidic hydrodynamic behavior in the past two decades has offered great promise for integrating multiple laboratory processes onto a single microfabricated chip. While throughput has been greatly increased and assay cost is now decreased dramatically thanks to many rapidly improving micro-total analysis systems (MTAS), challenges remain in several aspects of manufacture and design. Given the fact that MTAS applications involve electrokinetics (EK), studies of the interaction between the applied electric field and the charged fluids over the channel wall or around the suspended charges have become essential. In other words, information regarding the ion transport, coupling between the flow and two electric fields, turns out to be an academic subject worthy of intensive study in the field of electrohydrodynamics (EHD).

In microchannels of MTAS, the characteristic scales for the associated flows are slightly larger than 10 μm. Due to the resulting large surface-to-volume ratio,

Received 12 December 2008; accepted 13 February 2009.
Financial support provided by the National Science Council under Grants NSC97-2221-E-002-250-MY3, NSC97-2628-M-002-022, and CQSE project 97R0066-69 are gratefully acknowledged.
Address correspondence to Tony W. H. Sheu, Department of Engineering Science and Ocean Engineering, National Taiwan University, No. 1, Sec. 4, Roosevelt Road, Taipei 10617, Taiwan, Republic of China. E-mail: twhsheu@ntu.edu.tw

NOMENCLATURE

c_i	concentration	u	velocity component along x direction
c_p	specific heat at constant pressure	$\mathbf{u}$	velocity vector
D	dielectric constant	U_{ref}	reference velocity, m/s
D_i	diffusion coefficient of the ith species, m^2/s	v	velocity component along y direction
		z	valence of the ion
e	elementary charge, C	ε	permittivity of the buffer solution, C/mV
$\mathbf{E}$	strength of the applied electric field	ε_0	permittivity of vacuum, C/mV
f, f	source term	κ	$\equiv h^2/\lambda^2$
h	channel height	λ	electrical conductivity of the buffer solution, s/m
$\mathbf{I}$	electrical current density, C/sm^2		
k_b	Boltzmann constant, J/K	λ^*	debye length, m
k_1	coefficient of the diffusion term	ν	kinematic viscosity, m^2/s
n	buffer ion density, mol/m^3	ξ	surface zeta potential, V
n_0	ion density bulk solution, mol/m^3	ρ	density of the fluid, kg/m^3
N_0	Avagadro's number ($N_0 = 6.02 \times 10^{23}$)	ρ_e	space charge density
p	pressure	ϕ	externally applied electrical potential
q	Joule heat generation, W/m^3	Φ	$\equiv\phi + \psi$
Re	Reynolds number ($=U_{\text{ref}}h/\mu$)	ψ	electrical potential in electric double layer
T	absolute temperature, K		

Downloaded by [China Science & Technology University] at 02:33 26 February 2014

liquid fluids in microchannels, subjected to an externally applied electrical field, will be influenced by the interfacial effect due to, for example, the formation of an electric double layer (EDL) in an externally applied electric field. Near the charged surface, which is in contact with electrolyte, the EDL consists of a compact layer of immobile balancing charges and a diffuse layer of mobile ions. The thickness of the counterion shielding layer can be characterized by the Debye length, which typically has a length of 10 nm or less. The interface between the compact (or Stern) layer and the diffuse layer, in which the liquid velocity is zero under the zero pressure gradient condition, is called the shear plane. In the diffuse layer, the excess counterions can cause the fluid at rest to flow under the externally applied force. This phenomenon is referred to as electro-osmosis and was observed by Ruess in 1809 [1]. The bulk flow nature is now known to be a direct consequence of electro-osmosis, since moving ions can drag their surrounding fluids by virtue of the fluid viscosity. The microchannel flow in the EDL, which differs from the conventional Navier-Stokes flow, therefore warrants fundamental study.

Application of the electro-osmotic flow (EOF) theory [2] was limited to only some fields in the past. Thanks to emerging micro-electro-mechanical system (MEMS) techniques, breakthroughs toward utilizing an electro-osmotic flow in more complex microfluidic networks have been a great aid for loading, mixing, and flushing purposes. Due to the emerging lab-on-a-chip microfluidic devices, numerous experimental and computational studies have been carried out to enhance our understanding of the electro-osmotic phenomena observed in microchannels. Most of previous investigations addressed the hydrodynamic behavior, for which the velocity distribution takes a kind of plug flow. Very little attention has been paid to studying the natural consequence of an electric field applied on the conductive liquid. The inevitable formation of Joule heat in the electrohydrodynamic field not only can cause the electrolyte temperature to increase but can also result in a larger

Downloaded by [China Science & Technology University] at 02:33 26 February 2014

temperature gradient, which may dramatically affect the electro-osmotic flow, transport of the biosample, and sample separation. In addition to the low column separation efficiency, reduction of resolution, and loss of injected samples, flow instability in low-Reynolds-number electrokinetic flows with high gradients of electrical conductivity may be established inside the microchannel, which is subject to a strong electric field [3, 4].

With the advent of high-performance computing and better knowledge of EHD in the design of MTAS, numerical investigations of Joule heating effect on the electro-osmotic flow and the electrophonetic transport of solutes in microfluidic channels have become one of the focal points in the area of EOF [5–8]. The current study is aimed at elucidating some details of the formation of the electric double layer and its relation to the developed velocity boundary layer. The competition among the viscous force, pressure gradient force, and the electrokinetic force due to the EDL formed immediately adjacent to the bounding wall will be explored numerically.

The rest of this article is organized as follows. In Section 2, the coupling equations for the hydrodynamic, electrical, and thermal field variables are described at length. Energy generation due to Joule heating are taken into account in the energy equation. In addition to the inertia, viscous, and pressure gradient forces in the hydrodynamic system, the electrokinetic force is also considered in the equations of motion for the calculation of solute acceleration and, then, the flow velocity in the resulting electrohydrodynamic system. The locally analytic convection-diffusion reaction scheme applied to approximate the spatial derivative terms shown in the system of six coupled equations is described in Section 3 and then verified in Section 4. Discussion of the predicted results for the problem under current investigation is given in Section 5. Finally, some conclusions drawn from this study are given in Section 6.

2. WORKING EQUATIONS

The electrokinetic flow in a straight microchannel is considered to address the Joule heating effect on the electro-osmotic velocity. To this end, a full coupling of equations among the electric, hydrodynamic, and thermal fields is considered in this study. For an incompressible electrolyte fluid flow, subjected to an externally applied electric equation, the continuity equation and Navier-Stokes equations can be written in terms of the electrolyte density (ρ), hydrodynamic pressure (p), and velocity ($\mathbf{u}$) given below:

$$\nabla \cdot \mathbf{u} = 0 \tag{1}$$

$$\frac{\partial \mathbf{u}}{\partial t} + (\mathbf{u} \cdot \nabla)\mathbf{u} = -\frac{1}{\rho}\nabla p + \nu \nabla^2 \mathbf{u} + \mathbf{f} \tag{2}$$

In the above, $\mathbf{f}(\equiv \rho_e \mathbf{E})$ denotes the electrokinetic body force due to the formation of an electric double layer along the no-slip bounding surface [9]. Here, ρ_e denotes the local electric charge density. The strength of the applied electric field $\mathbf{E}$ is defined by the following negative gradient of the electrical potential Φ:

$$\mathbf{E} = -\nabla \Phi \tag{3}$$

Downloaded by [China Science & Technology University] at 02:33 26 February 2014

Under the steady-state assumption, Φ can be rigorously modeled by the following Poisson equation according to the theory of electrostatics:

$$\nabla^2(\varepsilon\,\Phi) = -\frac{\rho_e}{\varepsilon_0} \tag{4}$$

In the above, $\varepsilon_0(=8.854\times10^{-12}\ \mathrm{C/Vm})$ and ε denote the permittivity for the vacuum and fluid medium, respectively.

It is legitimate to separate Φ into the electrical potential ϕ due to an externally applied electric field and the zeta potential ψ (or electrokinetic potential). According to this decomposition, Eq. (4) can be rewritten as the sum of the following two equations [10]:

$$\nabla\cdot(\lambda\nabla\phi) = 0 \tag{5}$$

$$\nabla^2(\varepsilon\psi) = -\frac{\rho_e}{\varepsilon_0} \tag{6}$$

If the electrolyte under current investigation is classified to be symmetric and univalent, ρ_e can be represented by [10]

$$\rho_e = -\frac{2n_0ez}{\varepsilon_{\mathrm{ref}}}\sinh\left(\frac{ez\psi}{k_bT}\right) \tag{7}$$

In the above, $n_0(=6.02\times10^{20}\ 1/\mathrm{m}^3)$ is the density of positive or negative ion in the buffer, $e(=1.6\times10^{-19}\ C)$ denotes the electron charge, z is the valence ($\equiv1$). In Eq. (7), k_b is the Boltzmann constant ($=1.38\times10^{-23}$ J/K) and T is the absolute temperature. Under the above conditions, the Poisson-Boltzmann equation given below will be used in the present study [12]:

$$\nabla^2(\varepsilon\psi) = \frac{2n_0ez}{\varepsilon_0}\sinh\left(\frac{ez\psi}{k_bT}\right) \tag{8}$$

The Navier-Stokes equations subjected to an externally applied electric field $(-\partial\phi/\partial x, -\partial\phi/\partial y)$ and an electrokinetic field $(-\partial\psi/\partial x, -\partial\psi/\partial y)$ developed in the diffuse layer are

$$\rho\left(\frac{\partial u}{\partial t}+u\frac{\partial u}{\partial x}+v\frac{\partial u}{\partial y}\right) = -\frac{\partial p}{\partial x}+\frac{\partial}{\partial x}\left(\mu\frac{\partial u}{\partial x}\right)+\frac{\partial}{\partial y}\left(\mu\frac{\partial u}{\partial y}\right)-\rho_e\left(\frac{\partial\phi}{\partial x}+\frac{\partial\psi}{\partial x}\right) \tag{9}$$

$$\rho\left(\frac{\partial v}{\partial t}+u\frac{\partial v}{\partial x}+v\frac{\partial v}{\partial y}\right) = -\frac{\partial p}{\partial y}+\frac{\partial}{\partial x}\left(\mu\frac{\partial v}{\partial x}\right)+\frac{\partial}{\partial y}\left(\mu\frac{\partial v}{\partial y}\right)-\rho_e\left(\frac{\partial\phi}{\partial y}+\frac{\partial\psi}{\partial y}\right) \tag{10}$$

The reference quantities chosen to render the dimensionless variables in the current study are given by $x^*=x/H$, $y^*=y/H$, $t^*=U_{\mathrm{ref}}t/H$, $u^*=u/U_{\mathrm{ref}}$, $v^*=v/U_{\mathrm{ref}}$, $p^*=p/\rho U_{\mathrm{ref}}^2$, $\mu^*=\mu/\mu_{\mathrm{ref}}$, $\psi^*=ze\psi/k_bT$, $n_+^*=n_+/n_0$, $n_-^*=n_-/n_0$, $U_{\mathrm{ref}}=-\varepsilon_{\mathrm{ref}}\varepsilon_0\xi\Phi_{\mathrm{ref}}/\mu_{\mathrm{ref}}L$. The resulting dimensionless working equations, in addition to Eq. (1), are summarized as follows:

$$\frac{\partial}{\partial x}\left(\lambda\frac{\partial\phi}{\partial x}\right)+\frac{\partial}{\partial y}\left(\lambda\frac{\partial\phi}{\partial y}\right)=0 \tag{11}$$

$$\frac{\partial}{\partial x}\left(\varepsilon\frac{\partial\psi}{\partial x}\right)+\frac{\partial}{\partial y}\left(\varepsilon\frac{\partial\psi}{\partial y}\right)=\frac{2H^2z^2e^2n_0}{k_bT\varepsilon_{\mathrm{ref}}\varepsilon_0}\sinh(\psi) \tag{12}$$

$$\frac{\partial u}{\partial t}+u\frac{\partial u}{\partial x}+v\frac{\partial u}{\partial y}=-\frac{\partial p}{\partial x}+\frac{1}{\mathrm{Re}}\frac{\partial}{\partial x}\left(\mu\frac{\partial u}{\partial x}\right)+\frac{1}{\mathrm{Re}}\frac{\partial}{\partial y}\left(\mu\frac{\partial u}{\partial y}\right)+\frac{2Hzen_0\sinh(\psi)}{\rho U_{\mathrm{ref}}^2}\frac{\partial\phi}{\partial x}+\frac{2n_0k_bT\sinh(\psi)}{\rho U_{\mathrm{ref}}^2}\frac{\partial\psi}{\partial x} \tag{13}$$

$$\frac{\partial v}{\partial t}+u\frac{\partial v}{\partial x}+v\frac{\partial v}{\partial y}=-\frac{\partial p}{\partial y}+\frac{1}{\mathrm{Re}}\frac{\partial}{\partial x}\left[\mu(T)\frac{\partial v}{\partial x}\right]+\frac{1}{\mathrm{Re}}\frac{\partial}{\partial y}\left[\mu(T)\frac{\partial v}{\partial y}\right]+\frac{2Hzen_0\sinh(\psi)}{\rho U_{\mathrm{ref}}^2}\frac{\partial\phi}{\partial y}+\frac{2n_0k_bT\sinh(\psi)}{\rho U_{\mathrm{ref}}^2}\frac{\partial\psi}{\partial y} \tag{14}$$

In the above, Re is defined by $\rho U_{\mathrm{ref}}H/\mu_{\mathrm{ref}}$ and * has been omitted for the sake of brevity.

Within the mixed formulation, where the divergence-free constraint equation (1) is solved together with the momentum equations (13)–(14), inclusion of the constraint equation (1) will increase the matrix condition number and matrix size. To overcome this computational difficulty, we adopt the conventional segregated approach by reformulating the mass conservation equation in terms of the pressure by virtue of $(\partial/\partial x)$ (13) + $(\partial/\partial y)$ (14) and then employing Eq. (1). The resulting pressure Poisson equation, which is used in place of the mass conservation equation (1), can be derived as

$$\nabla^2p=\frac{\partial}{\partial x}\left[-\rho\left(\frac{\partial u}{\partial t}+u\frac{\partial u}{\partial x}+v\frac{\partial u}{\partial y}\right)+\frac{\partial}{\partial x}\left(\mu\frac{\partial u}{\partial x}\right)+\frac{\partial}{\partial y}\left(\mu\frac{\partial u}{\partial y}\right)-\rho_e\left(\frac{\partial\phi}{\partial x}+\frac{\partial\psi}{\partial x}\right)\right]+\frac{\partial}{\partial y}\left[-\rho\left(\frac{\partial v}{\partial t}+u\frac{\partial v}{\partial x}+v\frac{\partial v}{\partial y}\right)+\frac{\partial}{\partial x}\left(\mu\frac{\partial v}{\partial x}\right)+\frac{\partial}{\partial y}\left(\mu\frac{\partial v}{\partial y}\right)-\rho_e\left(\frac{\partial\phi}{\partial y}+\frac{\partial\psi}{\partial y}\right)\right] \tag{15}$$

For calculating a physically more plausible steady-state temperature in the electro-osmotic microflow field, Joule heat will be considered in the following energy equation:

$$\rho c_p\left(u\frac{\partial T}{\partial x}+v\frac{\partial T}{\partial x}\right)=\frac{\partial}{\partial x}\left(k_1\frac{\partial T}{\partial x}\right)+\frac{\partial}{\partial y}\left(k_1\frac{\partial T}{\partial y}\right)+q \tag{16}$$

where c_p is the specific heat capacity, k_1 is the thermal conductivity, and q is the Joule heat. Note that heat generation due to viscous dissipation is normally quite small and can be neglected. Thanks to Ohm's law, the energy generation due to Joule heating can be expressed as $q=\mathbf{I}\cdot\mathbf{I}/\lambda$ [5], where $\mathbf{I}$ denotes the electrical current density. In the current study, the electrical current density results from $\mathbf{E}\lambda$, which is due to the electric field applied to the conductive solution, and $\rho_e\mathbf{u}$, which results from the net charged density moving together with the fluid flow. In other words, the electrical current density $\mathbf{I}$ can be expressed as

$$\mathbf{I}=\rho_e\mathbf{u}+\lambda\mathbf{E} \tag{17}$$

Downloaded by [China Science & Technology University] at 02:33 26 February 2014

Downloaded by [China Science & Technology University] at 02:33 26 February 2014

Table 1 Summary of transport equations in Eq. (20)

	Continuity equation	Energy equation	x-Momentum equation	y-Momentum equation	Electric equation	Zeta potential
$\bar{\phi}$	p	T	u	v	ϕ	ψ
Γ	1	$\frac{k_1}{\mathrm{Pr}\cdot\mathrm{Re}}$	$\frac{\mu}{\mathrm{Re}}$	$\frac{\mu}{\mathrm{Re}}$	λ	ε
f	$-\left(\frac{\partial u}{\partial x}\right)^2-\left(\frac{\partial v}{\partial y}\right)^2-2\frac{\partial u}{\partial x}\frac{\partial v}{\partial y}+\frac{1}{\mathrm{Re}}\left[\frac{\partial \mu}{\partial x}\left(\frac{\partial^2 u}{\partial x^2}+\frac{\partial^2 u}{\partial y^2}\right)+\frac{\partial \mu}{\partial y}\left(\frac{\partial^2 v}{\partial x^2}+\frac{\partial^2 v}{\partial y^2}\right)\right]$ $+\frac{\partial}{\partial x}\left[\frac{2Hzen_0\sinh(\psi)}{\rho U_{\mathrm{ref}}^2}\frac{\partial \phi}{\partial x}+\frac{2n_0k_bT\sinh(\psi)}{\rho U_{\mathrm{ref}}^2}\frac{\partial \psi}{\partial x}\right]$ $+\frac{\partial}{\partial y}\left[\frac{2Hzen_0\sinh(\psi)}{\rho U_{\mathrm{ref}}^2}\frac{\partial \phi}{\partial y}+\frac{2n_0k_bT\sinh(\psi)}{\rho U_{\mathrm{ref}}^2}\frac{\partial \psi}{\partial y}\right]$	$\frac{H\left[u\rho_e-\left(\frac{\partial \phi}{\partial x}\right)\lambda(T)\right]^2+H\left[v\rho_e-\left(\frac{\partial \phi}{\partial y}\right)\lambda(T)\right]^2}{\rho c_p U_{\mathrm{ref}}(T_0-T_{\mathrm{ref}})\lambda(T)}$	$\frac{2Hzen_0\sinh(\psi)}{\rho U_{\mathrm{ref}}^2}\frac{\partial \phi}{\partial x}+\frac{2n_0k_bT\sinh(\psi)}{\rho U_{\mathrm{ref}}^2}\frac{\partial \psi}{\partial x}$	$\frac{2Hzen_0\sinh(\psi)}{\rho U_{\mathrm{ref}}^2}\frac{\partial \phi}{\partial y}+\frac{2n_0k_bT\sinh(\psi)}{\rho U_{\mathrm{ref}}^2}\frac{\partial \psi}{\partial y}$	0	$\frac{2H^2z^2e^2n_0}{k_bT\varepsilon_{\mathrm{ref}}\varepsilon_0}\sinh(\psi)$

Substituting Eq. (17) for **I** into Ohm's law and then into Eq. (16), we can derive the energy equation as

$$\rho c_p\left(\frac{\partial T}{\partial t}+u\frac{\partial T}{\partial x}+v\frac{\partial T}{\partial y}\right)=\frac{\partial}{\partial x}\left(k_1\frac{\partial T}{\partial x}\right)+\frac{\partial}{\partial y}\left(k_1\frac{\partial T}{\partial y}\right)+\frac{(u\rho_e+E_x\lambda)^2+(v\rho_e+E_y\lambda)^2}{\lambda} \tag{18}$$

For the chosen normalization quantities, given by $T^*=(T-T_{\text{ref}})/(T_0-T_{\text{ref}})$ and $k^*=k_1(T)/k_{\text{ref}}$, the dimensionless energy equation which includes the heat source due to Joule heating is derived as follows:

$$\frac{\partial T}{\partial t}+u\frac{\partial T}{\partial x}+v\frac{\partial T}{\partial y}=\frac{1}{\text{Pr Re}}\left\{\frac{\partial}{\partial x}\left[k_1(T)\frac{\partial T}{\partial x}\right]+\frac{\partial}{\partial y}\left[k_1(T)\frac{\partial T}{\partial y}\right]\right\}+\frac{H(u\rho_e+E_x\lambda)^2+H(v\rho_e+E_y\lambda)^2}{\rho c_p U_{\text{ref}}(T_0-T_{\text{ref}})\lambda} \tag{19}$$

Prior to describing the discretization scheme and the solution algorithm for solving the electrohydrodynamic equations in microchannels, the conservation equations for incompressible electrolyte fluid flow with the electro-osmotic body force, the Laplace equation for external electric field, the Poisson-Boltzmann equation for zeta potential, and the conservation equation for energy, with the inclusion of energy generation due to Joule heating, is cast into the following generalized form for all field variables:

$$\bar{\phi}_t+u\bar{\phi}_x+v\bar{\phi}_y=\Gamma\nabla^2\bar{\phi}+f \tag{20}$$

The definitions for $\bar{\phi}$, Γ, and f are tabulated in Table 1.

3. NUMERICAL MODEL

The model equation which can represent each of the electrohydrodynamic equations derived in the previous section is as follows:

$$\bar{\phi}_t+u\bar{\phi}_x+v\bar{\phi}_y-k\nabla^2\bar{\phi}+c\bar{\phi}=f \tag{21}$$

For simplicity, this convection-diffusion-reaction (CDR) differential equation is solved subject to a specified boundary value of $\bar{\phi}$. In the above, k and c denote the diffusion coefficient and the reaction coefficient, respectively. In what follows, the values for u, v, k, and c are assumed to be uniform. By virtue of the operator splitting method of Peaceman and Rachford [13], the solution for Eq. (21) is sought from the following equations, which are applied respectively in the predictor and corrector steps:

$$u\bar{\phi}_x^*-k\bar{\phi}_{xx}^*+c\bar{\phi}^*=f_1 \tag{22}$$

$$v\bar{\phi}_y^{n+1}-k\bar{\phi}_{yy}^{n+1}+c\bar{\phi}^{n+1}=f_2 \tag{23}$$

In the above, $f_1=f^*-v\bar{\phi}_y^n+k\bar{\phi}_{yy}^n$ and $f_2=f^{n+1}-u\bar{\phi}_x^*+k\bar{\phi}_{xx}^*$

Downloaded by [China Science & Technology University] at 02:33 26 February 2014

Downloaded by [China Science & Technology University] at 02:33 26 February 2014

As Eqs. (22)–(23) reveal, the key to predict the two-dimensional CDR equation (21) depends on the discretization scheme developed for the following equation:

$$u\bar{\phi}_x - k\bar{\phi}_{xx} + c\bar{\phi} = \bar{f} \tag{24}$$

For illustrative purposes, $\bar{f}$ is assumed to be a known value. Our strategy of approximating (24) is to employ its general solution,

$$\bar{\phi}(x) = c_1 e^{\lambda_1 x} + c_2 e^{\lambda_2 x} + \frac{\bar{f}}{c} \tag{25}$$

where $\lambda_{1,2} = u \pm \sqrt{u^2 + 4ck}/2k$, and c_1 and c_2 are two constants. The terms other than the diffusive term in Eq. (24) are approximated by the center-like scheme. The discrete equation at an interior node i for (24) can therefore be expressed as

$$\left(-\frac{u}{2h} - \frac{m}{h^2} + \frac{c}{6}\right)\bar{\phi}_{i-1} + 2\left(\frac{m}{h^2} + \frac{c}{3}\right)\bar{\phi}_i + \left(-\frac{u}{2h} - \frac{m}{h^2} + \frac{c}{6}\right)\bar{\phi}_{i+1} = \bar{f} \tag{26}$$

where h is the mesh size. The exact solutions given by $\bar{\phi}_{i+1} = c_1 e^{\lambda_1 h} e^{\lambda_1 x_i} + c_2 e^{\lambda_2 h} e^{\lambda_2 x_i} + \bar{f}/c$, $\bar{\phi}_i = c_1 e^{\lambda_1 x_i} + c_2 e^{\lambda_2 x_i} + \bar{f}/c$, and $\bar{\phi}_{i-1} = c_1 e^{-\lambda_1 h} e^{\lambda_1 x_i} + c_2 e^{-\lambda_2 h} e^{\lambda_2 x_i} + \bar{f}/c$ are then substituted into Eq. (26) to get the following closed-form expression for the coefficient m shown in Eq. (26) [14]:

$$m = h^2\left[\frac{(c/3) + (c/6)\ \cosh(\bar{\lambda}_1)\cosh(\bar{\lambda}_2) + (u/2h)\ \sinh(\bar{\lambda}_1)\cosh(\bar{\lambda}_2)}{\cosh(\bar{\lambda}_1)\cosh(\bar{\lambda}_2) - 1}\right] \tag{27}$$

where $(\bar{\lambda}_1, \bar{\lambda}_2) = \left[uh/2k, \sqrt{(uh/2k)^2 + ch^2/k}\right]$.

On physical grounds, $-\nabla p$ shown in the equations of motion should be discretized by a centered scheme. However, such an approximation of $\partial p/\partial x$ or $\partial p/\partial y$ in nonstaggered grids can result in spurious even–odd oscillations [15]. Therefore, it is essential to suppress these erroneous checkerboarding pressures when solving the incompressible viscous equations in collocated grids. To circumvent the even–odd decoupling problem, $M_j (\equiv h\bar{\phi}_x)$ and $N_j (\equiv^2 \bar{\phi}_{xx})$ are calculated implicitly from the following two implicit equations (16):

$$\begin{aligned}\alpha_0 M_{j+1} + \beta_0 M_j + \gamma_0 M_{j-1} = {} & a_0\left(\bar{\phi}_{j+2} - \bar{\phi}_{j+1}\right) + b_0\left(\bar{\phi}_{j+1} - \bar{\phi}_j\right) \\ & + c_0\left(\bar{\phi}_j - \bar{\phi}_{j-1}\right) + d_0\left(\bar{\phi}_{j-1} - \bar{\phi}_{j-2}\right)\end{aligned} \tag{28}$$

and

$$\alpha_1 N_{j+1} + \beta_1 N_j + \gamma_1 N_{j-1} = a_1\bar{\phi}_{j+2} + b_1\bar{\phi}_{j+1} + c_1\bar{\phi}_j + d_1\bar{\phi}_{j-1} + e_1\bar{\phi}_{j-2} \tag{29}$$

Provided that $(\alpha_0, \beta_0, \gamma_0, a_0, b_0, c_0, d_0, e_0) = \left(\frac{1}{5}, \frac{3}{5}, \frac{1}{5}, \frac{1}{60}, \frac{29}{60}, \frac{29}{60}, \frac{1}{60}\right)$ and $(\alpha_1, \beta_1, \gamma_1, a_1, b_1, c_1, d_1, e_1) = \left(1, \frac{11}{2}, 1, \frac{3}{8}, 6, -\frac{51}{4}, 6, \frac{3}{8}\right)$, the approximated equations for $\bar{\phi}_x$ and $\bar{\phi}_{xx}$ can be shown to accommodate sixth-order accuracy.

The implicit equations for M and N at the nodes located immediately adjacent to the boundary can be derived by specifying $d_0 = e_1 = 0$ and $a_0 = a_1 = 0$ at the nodes

Downloaded by [China Science & Technology University] at 02:33 26 February 2014

next to the left and the right boundaries, respectively. The values for $(\alpha_0, \beta_0, \gamma_0, a_0, b_0, c_0, d_0, e_0) = \left(\frac{3}{10}, \frac{3}{5}, \frac{1}{10}, \frac{1}{30}, \frac{19}{30}, \frac{1}{3}, 0\right)$ and $\left(\frac{1}{10}, \frac{3}{5}, \frac{3}{10}, 0, \frac{1}{3}, \frac{19}{30}, \frac{1}{30}\right)$ can be derived analytically at the nodal points next to the left and the right boundaries, respectively, by expanding the terms shown in (28) in Taylor series. Similarly, the coefficients shown in (29) for N at the node j can be exactly derived as (α_1, β_1, γ_1, a_1, b_1, c_1, d_1, e_1) = (1, 10, 1, 0, 12, −24, 12, 0).

For effectively solving the incompressible momentum equations, which are coupled with the transport equations for energy, electric field, and zeta potential, we apply the regularized solution algorithm proposed in [17]. The main idea of this iterative algorithm is to replace the incompressible constraint equation with the differential equation derived from Eq. (15). Refer to [17] for some details about the currently applied divergence free compensated (DFC) solution algorithm.

4. VERIFICATION STUDY

For the sake of validation, the electro-osmotic/pressure-driven flow problem of Dutta and Breskok [18] is investigated in a straight channel. The channel height h is much smaller than the channel width. The resulting two-dimensional-like steady-state channel flow is assumed to be fully developed. The resulting dimensionless streamwise momentum equation, subject to the dimensionless electro-osmotic potential ψ, can be simplified as [18]

$$\frac{\partial p^*}{\partial \xi} = \frac{\partial^2 U}{\partial \eta^2} \tag{30}$$

where $U = u/U_{\text{ref}}$, $p^* = ph/\mu U_{\text{ref}}$, $\xi = x/h$, and $\eta = y/h$. Note that ψ^* is governed by $d^2\psi^*/d\eta^2 = \beta \sinh(\alpha\psi^*)$, where α is the ionic energy parameter and $\beta[\equiv (wh)^2/\alpha]$ is associated with the Debye-Hückel parameter $w(=1/\lambda^*)$ or the Debye length λ^*. For this problem, the electro-osmotic potential has been analytically derived in [12] as follows:

$$\psi^* = \frac{4}{\alpha} \tanh^{-1}\left[\tanh\left(\frac{\alpha}{4}\right) \exp(-\sqrt{\alpha\beta}\eta^*)\right] \tag{31}$$

where $\eta^*(\equiv 1 - |\eta|)$ is the normalized distance from the wall. It can be observed from Figure 1 that the predicted zeta potential agrees well with the above exact solution.

Under the nonzero pressure gradient condition, the linear equation (30) can be integrated to yield the following dimensionless velocity profile in the mixed electro-osmotic/pressure gradient flow by virtue of the superposition principle [18]:

$$U(\eta) = -\frac{1}{2}\frac{dp^*}{d\xi}(1 - \eta^2) + [1 - \psi^*(\eta)] \tag{32}$$

In the case of zero pressure gradient, Eq. (31) turns out to be the one studied previously by Burgreen and Nakache [19]. Note that the case investigated at $dp^*/d\xi = 0$ corresponds to pure pluglike flow, which has been experimentally observed in [18].

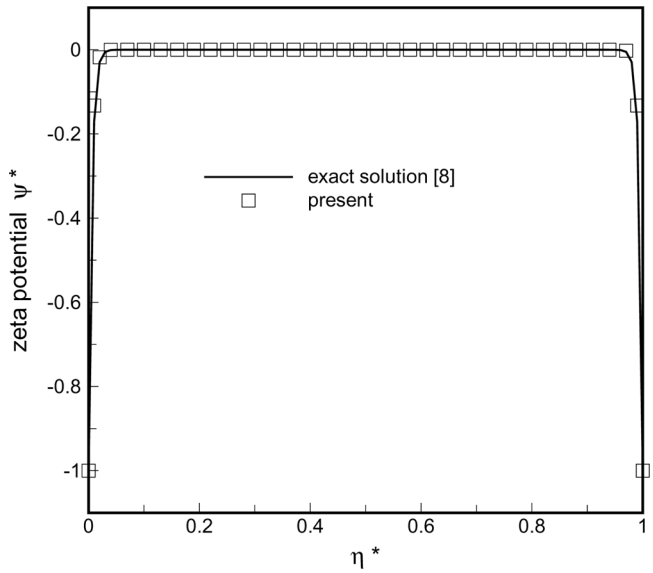

Figure 1. Comparison of the predicted and analytic zeta potentials against η^*.

Our results are computed at $\alpha = 1$ and $\beta = 10^4$ for the cases with favorable pressure gradients $\chi(\equiv dp^*/d\xi = -0.5$ and $-1.0)$, adverse pressure gradients $(= dp^*/d\xi =$ 0.5 and 1.0), and zero pressure gradient. As can be seen from Figure 2, the predicted velocity distributions plotted against η for the mixed electro-osmotic/

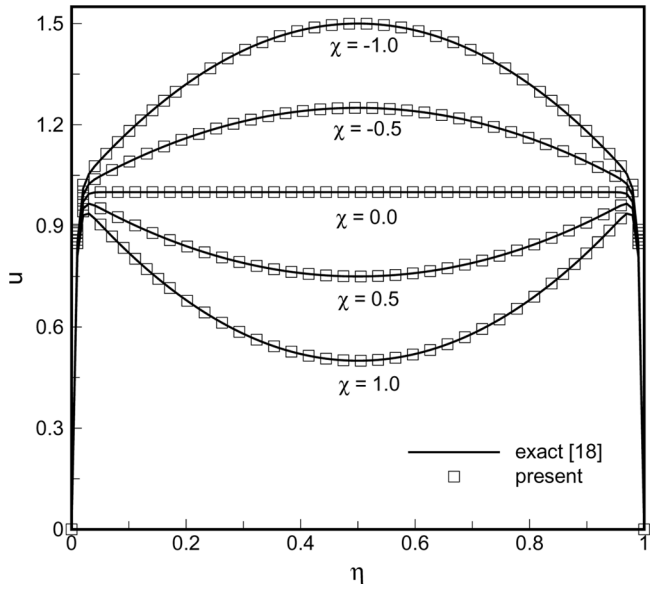

Figure 2. Comparison of the predicted and analytic velocity profiles for cases with different values of the pressure gradient χ.

Downloaded by [China Science & Technology University] at 02:33 26 February 2014

pressure-driven flows compare favorably with the analytic solutions, given by (32), obtained at the five chosen values of $dp^*/d\xi$. The present method, as a result, is verified owing to the perfect agreement between the predicted and the analytic zeta potentials and the predicted velocity distributions shown in Figures 1 and 2, respectively.

5. DISCUSSION OF RESULTS

We consider in this study the electro-osmotic fluid flow bounded by the silica walls at $y = \pm 0.5$. These glass surfaces, which are immersed in an aqueous solution, are negatively charged through the hydration schematic in Figure 3. The resulting charged surfaces tend to attract some positive ions (or counterions) in the direction toward the no-slip wall and therefore form a Stern layer (or compact layer), which shields the surface charges. The negative charges in the solution, on the other hand, will be repelled from the two walls. Due to thermal motion, ions of opposite charge to the surface are not bound to the wall surface but rather remain dispersed and mobile in the vicinity of the two parellel walls. Such a spatial charge separation is the outcome of the electrostatic force and the thermal motion in the respective Stern layer and diffuse layer (or Gouy-Chapman layer). As the result of the electric double-layer formation, one consequence of the space charge distribution is that the spatially varying electric potential within it is changed from zero at a location far from the surface to its maximum magnitude in regions very near the surface. An electric field is then established near the solid–liquid interface due to attraction and repulsion of the positive charges.

Since the electrokinetic phenomenon is essential in microfluidics, we are motivated to understand how the applied electric field and the established electrical potential field in the solution due to attracting and repelling charges to/from the wall can affect the hydrodynamic behavior in the microchannel. The immobile positive ions are seen in the compact Stern layer, and the mobile ions show their presence in the diffuse layer. We also want to know the distance, measured from the wall, beyond which the surface charges can no longer affect the ion distribution in the solution. In other words, we aim to compare the simulated Debye length and the value of $\lambda^* = (8\pi n_0 e^2 z^2 / D k_b T)^{-1/2}$, where n_0 is the ion density in the bulk solution, k_b is the Boltzmann constant, and D is the dielectric constant [18].

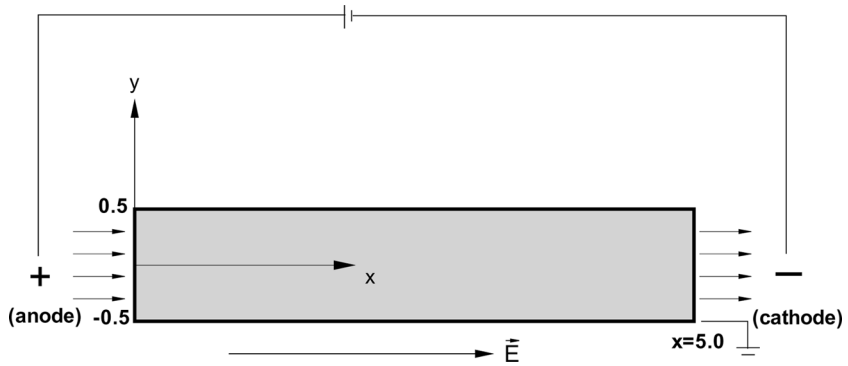

Figure 3. Schematic of the investigated microchannel.

Downloaded by [China Science & Technology University] at 02:33 26 February 2014

Downloaded by [China Science & Technology University] at 02:33 26 February 2014

In a straight channel of width 1×10^{-4} m and length 5×10^{-4} m, an electric potential with unit voltage is applied at the left entrance and the right exit is grounded. With this externally applied electric field, the positive ions within the EDL tend to advect toward the cathode end. Such ion movement along the streamwise direction can, in turn, result in an electrically driven flow due to fluid viscosity. The Debye length is set at 4.3×10^{-7} m, corresponding to the ion concentration of NaCl at 298°K. We consider in this study the following physical properties for NaCl: density (=1,000 kg/m^3), concentration (=10^{-4} M), dielectric constant (=78.4), and specific heat (=4,180 J/kg K).

The working equations are solved sequentially subject to the following boundary conditions prescribed at the channel inlet, channel outlet, and the no-slip walls, respectively:

Inlet:

$$T = 0 \qquad \phi = 1 \qquad \frac{\partial \psi}{\partial x} = 0 \qquad \frac{\partial u}{\partial x} = \frac{\partial v}{\partial x} = 0$$
$$\frac{\partial p}{\partial x} = -\frac{\partial u}{\partial t} - v\frac{\partial u}{\partial y}\frac{1}{\mathrm{Re}}\left(\frac{\partial \mu}{\partial y}\frac{\partial u}{\partial y} + \mu\frac{\partial^2 u}{\partial y^2}\right) + f_1 \tag{33}$$

Outlet:

$$\frac{\partial T}{\partial x} = 0 \qquad \phi = 0 \qquad \frac{\partial \psi}{\partial x} = 0 \qquad \frac{\partial u}{\partial x} = \frac{\partial v}{\partial x} = 0 \qquad p = 0 \tag{34}$$

Wall:

$$\psi = \xi_0 \qquad u = v = 0 \qquad \frac{\partial \phi}{\partial y} = 0 \qquad \frac{\partial p}{\partial y} = 0 \qquad \frac{\partial T}{\partial y} = 0 \tag{35}$$

The effect of Joule heat on the EOF, which exists between the silica glasses, will be discussed. According to the physical properties and the definitions of Re, Pr (Prandtl number $\equiv \nu\rho c_p/k_1$), and Sc (Schmidt number $\bar{\mu}/\rho_f D$), the current simulation is carried out at $\mathrm{Re} = 0.23$, $\mathrm{Pr} = 5.95$, and $\mathrm{Sc} = 42{,}661$ (or Peclet number $\mathrm{Pe} = \mathrm{Re} \cdot \mathrm{Sc} = 9{,}812.03$) in a uniform mesh with $1{,}001 \times 101$ nodal points for the case with electrical conductivity $\lambda = 1.264 \times 10^{-6}$ (obtained at room temperature) and the prescribed zeta potential $\psi = -1$.

Discussion of results begins with the comparison of streamwise velocities for the cases with/without taking Joule heat into account. For this reason, we plot in Figure 4 the x-component velocity against the transverse coordinate y at, for example, $x = 2.5$. It can be seen clearly from this figure that both velocity profiles have a marked velocity gradient near the wall. The reason for such a sharp velocity profile is the rapidly varying electrokinetic force $-\rho_e[(\partial\phi/\partial x) + (\partial\psi/\partial y)]$, plotted in Figure 5, along the transverse direction. It is worth noting that the electrokinetic force due to the electrokinetic potential [or $-\rho_e(\partial\psi/\partial x)$] prevailingly dominates the force due to the externally applied electric field [or $-\rho_e(\partial\phi/\partial x)$]. Also, the electrokinetic force in the y direction is negligibly small in comparison with $-\rho_e(\partial\psi/\partial x)$. Due to the predicted positive electrokinetic force over the entire range of y, the magnitude of u for the case with consideration of Joule heat effect is larger than that

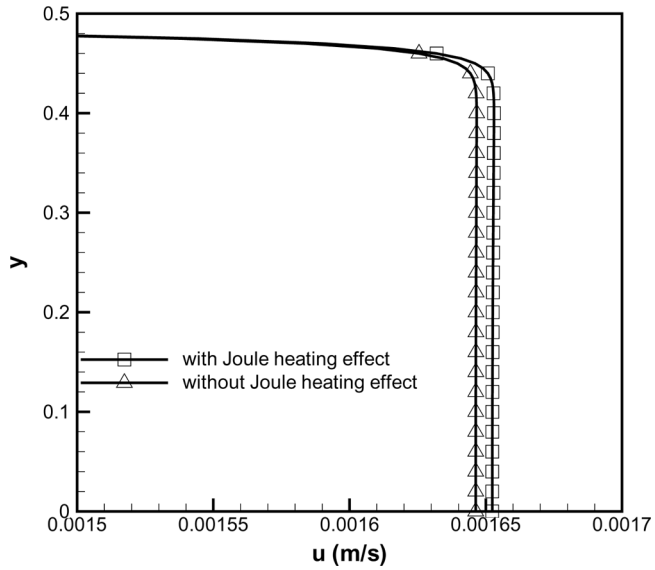

Figure 4. Comparison of the streamwise velocity profiles at $x = 2.5$ for cases with/without consideration of Joule heat.

without taking the Joule heating into account. Note that the electrokinetic body force shown in Figure 5 quickly reaches the constant value in the opposite direction toward the wall. The pluglike flow profile featured with uniform velocity in the channel core is therefore predicted.

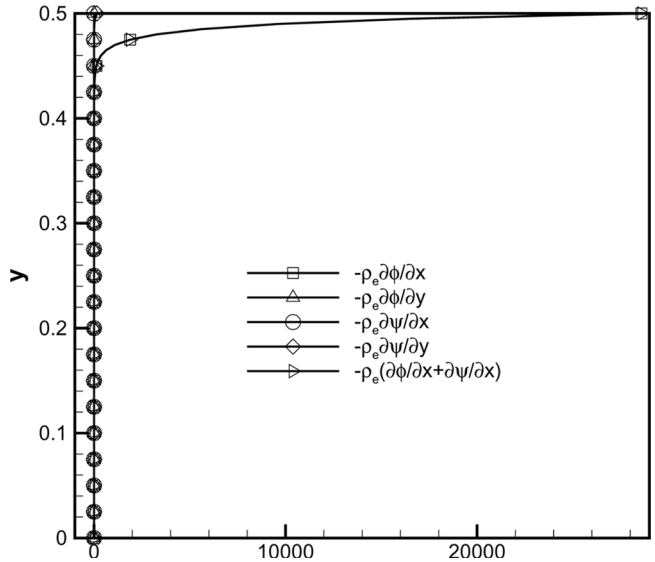

Figure 5. The plots of $-\rho_e(\partial\phi/\partial x)$, $-\rho_e(\partial\phi/\partial y)$, $-\rho_e(\partial\psi/\partial x)$ and $-\rho_e(\partial\psi/\partial y)$ against y at $x = 2.5$ for the case with Joule heating.

Downloaded by [China Science & Technology University] at 02:33 26 February 2014

Downloaded by [China Science & Technology University] at 02:33 26 February 2014

We also plot the temperature profiles $T(y)$ predicted at $x = 2.5$ in Figure 6 with/without the Joule heat being taken into account. The difference between the two predicted temperatures is due mainly to the Joule heat $\mathbf{I} \cdot \mathbf{I}/\lambda$. For this reason, it is necessary to plot the Joule heat against y in Figure 7. The Joule heat is theoretically positive, and thus can be considered as a heat source adding to the EOF system, thereby causing the temperature in the microchannel to rise.

It is also interesting to know how the temperature varies along the streamwise direction. For this reason, we plot the predicted T along the channel central line in Figure 8. It can be seen from this figure that from the inlet the predicted temperature keeps increasing with a larger slope in the channel upstream, followed by a slowly varying profile in the direction toward the channel exit. This monotonically increasing temperature profile coincides with the streamwise distribution of the Joule heat plotted in Figure 9. The monotonically increasing temperature near the channel inlet is due partly to the production of Joule heat, which is mainly advected downstream with the prevailing streamwise velocity shown in Figure 4, and partly by the thermal diffusion process dissipated along all the spatial directions.

To show that the presently investigated flow is characterized as electro-driven flow rather than pressure-driven flow, we plot the ratio of $-\rho_e(\partial\phi/\partial x)/-(\partial p/\partial x)$ against y at several chosen streamwise locations $x = 0$, 0.25, 1, and 4. Clearly seen from Figure 10 is that along the streamwise direction the electrokinetic force dominates the pressure gradient force. Due to the dramatic difference between these two external forces shown in the x-momentum equation, one can expect that the pluglike EOF velocity plotted in Figure 11 differs from the parabolic-like

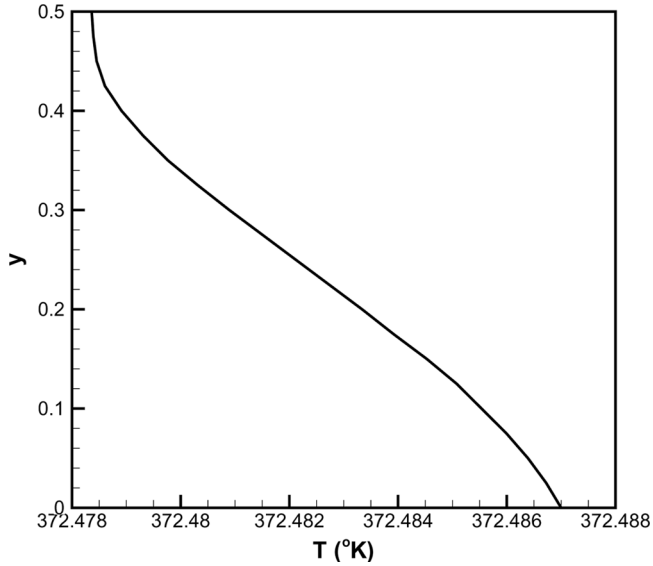

Figure 6. Predicted temperature profile $T(2.5, y)$ for the case with/without Joule heating effect at $\lambda = 1.264 \times 10^{-4}$.

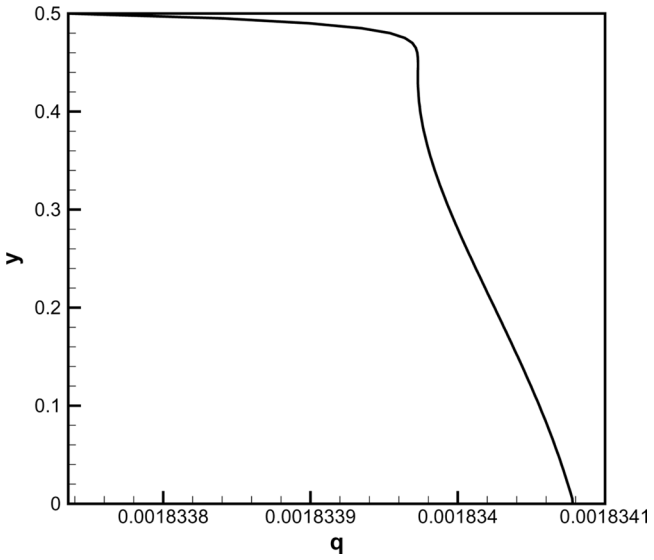

Figure 7. Predicted Joule heat q at $x = 2.5$ along the y direction.

pressure-driven velocity profile. For the sake of completeness, we also plot the u-velocity profiles at $x = 0$, 1, 2, 2.5, 4, and 5 in Figure 12.

For purposes of exploring the flow details, we define the edge of the velocity boundary layer at a y location where the velocity magnitude is equal to $0.99 \times u(x, y = 0)$. Following this definition, we plot the velocity boundary layer along the x direction in Figure 13.

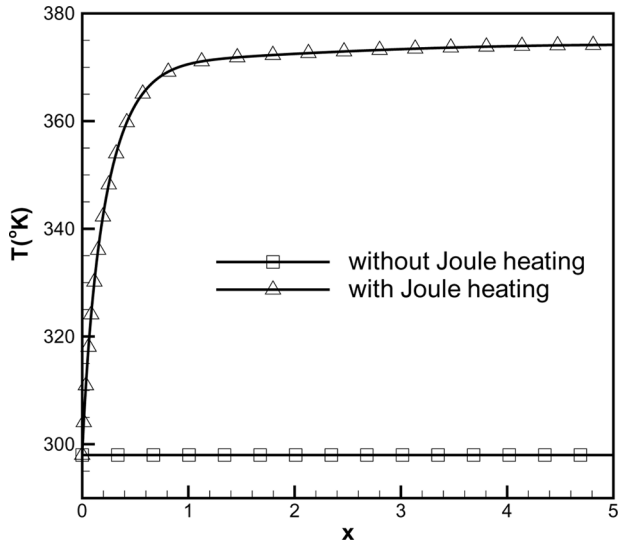

Figure 8. Predicted temperature profiles $T(x, 0)$ against streamwise coordinate x for cases with/without Joule heat.

Downloaded by [China Science & Technology University] at 02:33 26 February 2014

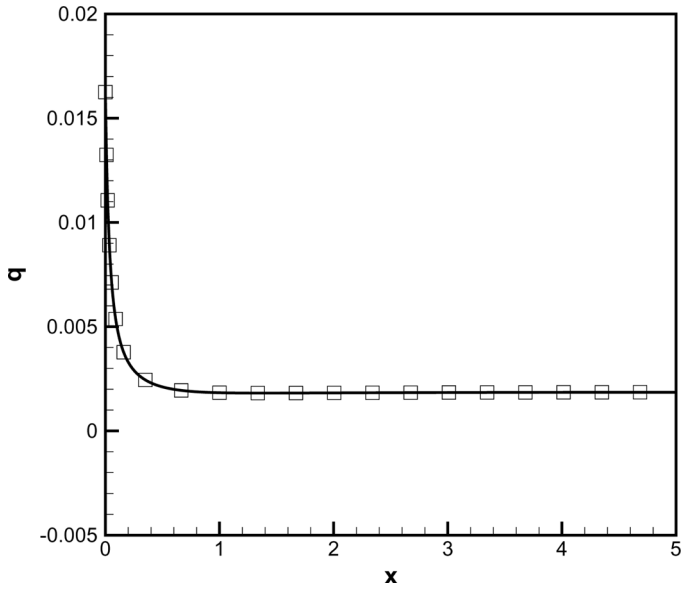

Figure 9. Predicted Joule heat q along the streamwise direction x along the plane of symmetry.

Adjacent to the investigated microchannel, there exists a Stern layer with a thickness equal to 9.8×10^{-11} m. A shear plane is normally considered as the edge of the Stern layer, over which is the diffuse layer. To characterize the thickness of the diffuse layer, one defines the Debye length, along which is the shear plane

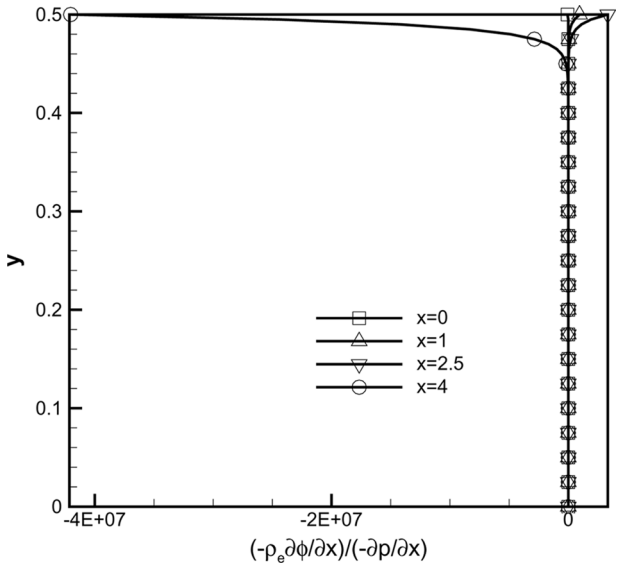

Figure 10. Plots of the ratio of the electrokinetic and pressure gradient forces against y at $x = 0$, 1, 2.5, and 4.

Downloaded by [China Science & Technology University] at 02:33 26 February 2014

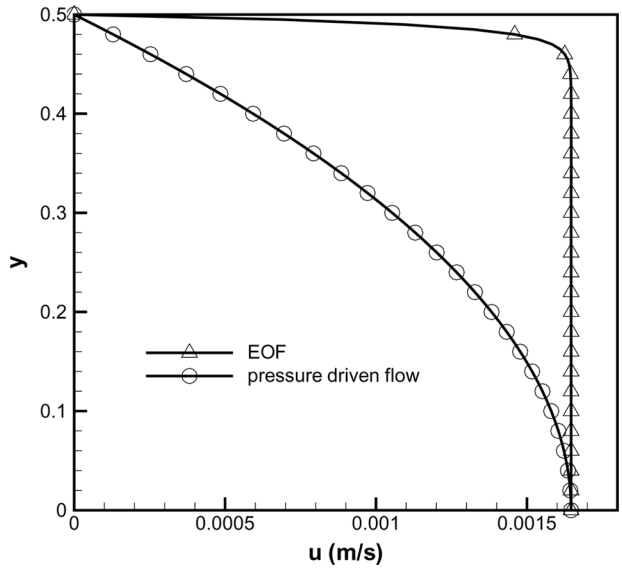

Figure 11. Comparison of predicted velocity profiles $u(y)$ at $x = 2.5$ for electro-driven and pressure-driven flows.

(or the interface between the Stern layer and the diffuse layer). This physically important length can be considered as the length, measured from the wall, at which the zeta potential is equal to $\psi_{wall}/\exp$. To determine the edge of the diffuse layer, we plot the predicted zeta potentials in Figure 14 along the streamwise direction. The line connecting the location y^*, where the zeta potentials $\psi(x, y^*)$ have the value

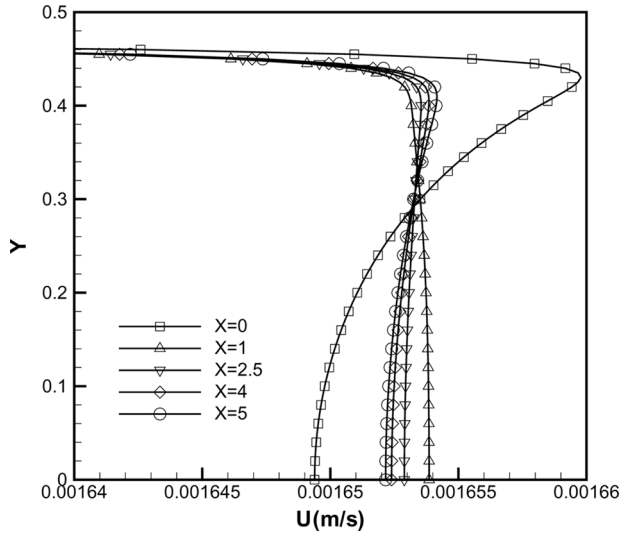

Figure 12. Predicted EOF velocity profiles $u(x, y)$ at several selected streamwise locations.

Downloaded by [China Science & Technology University] at 02:33 26 February 2014

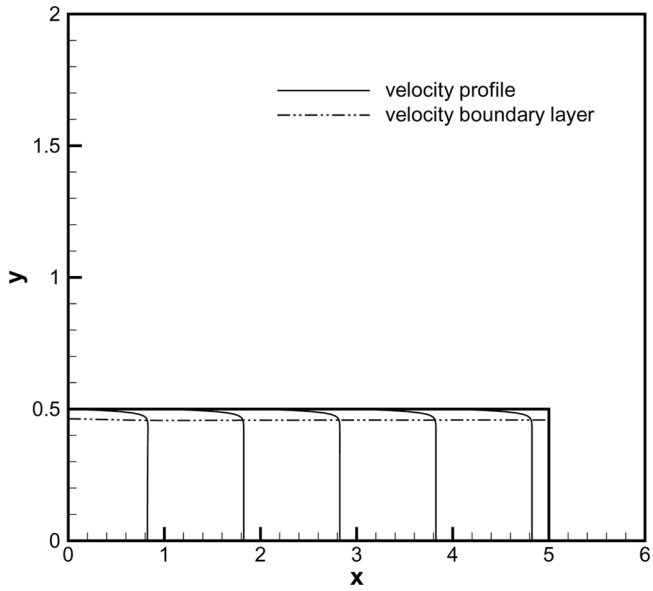

Figure 13. Predicted velocity profile and velocity boundary layer.

of ψ_{wall}/exp, is plotted in Figure 15. The electric double layer mentioned earlier is another physically important characteristic length in the EOF. For this reason, we are also motivated to plot the predicted EDL at which the zeta potential has been decreased to zero in Figure 15.

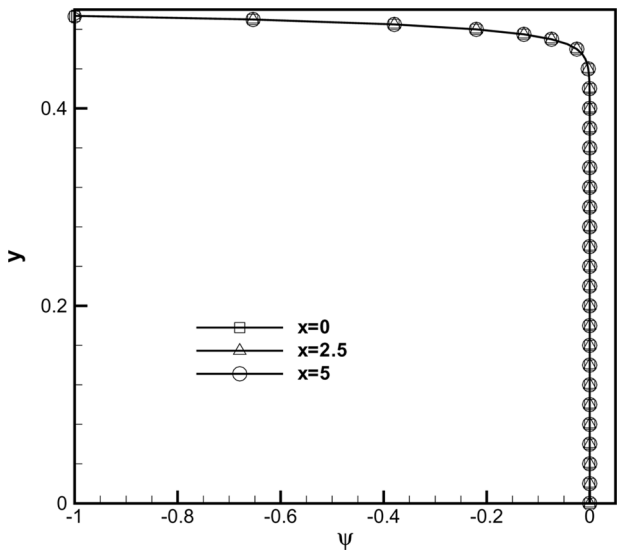

Figure 14. Plots of predicted zeta potentials $\psi(x, y)$ at $x = 0$, 2.5, and 5.

Downloaded by [China Science & Technology University] at 02:33 26 February 2014

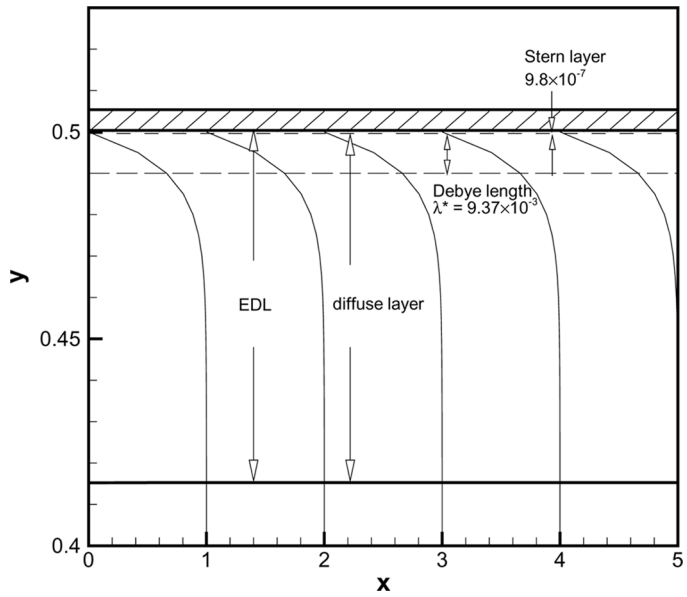

Figure 15. Predicted zeta potential distributions (at $x = 0, 1, 2, 3, 4$), diffuse layer, and electric double layer.

6. CONCLUDING REMARKS

In this study, mixed electro-osmotic/pressure-driven flow has been studied numerically in a straight channel, with emphasis on the Joule heat in the equations of motion. Nonlinear EHD behaviors, resulting from the triple coupling of the hydrodynamic, thermal, and electrical fields and the specified temperature-dependent properties for the fluid viscosity, thermal conductivity, electrical permittivity, and conductivity of the buffer solution, have been analyzed in nonstaggered grids. Within the context of the predictor-corrector two-step method, the locally analytic one-dimensional convection-diffusion reaction scheme has been applied in each operator-splitting step to capture the sharply varying field variables. The predicted results from the employed discretization scheme for solving the hydrodynamic, thermal, and electrical field equations have been verified to have good agreement with the analytical solutions. Conclusions drawn from the predicted solutions for the test problem are as follows. Electrokinetic force was found to be prevailing in the diffuse layer and decreases rapidly to zero in the direction toward the channel core, resulting in a sharp velocity profile near the channel wall and a plateau-like velocity profile in the channel core. The theoretical reason for this distinguishing velocity profile is explained in this study. Since the region located immediately adjacent to the channel wall plays a dominant role in determining the EOF phenomena, we have plotted the edges of the diffuse layer and the velocity boundary layer, in addition to the profile capable of exhibiting the Debye length.

REFERENCES

1. F. F. Reuss, Charge-Induced Flow, *Proc. Imperial Society of Naturalists Moscow*, vol. 3, pp. 327–344, 1809.

Downloaded by [China Science & Technology University] at 02:33 26 February 2014

2. G. Wiedemann, First Quantitative Study of Electrical Endosmose, *Pogg. Ann.*, vol. 87, p. 321, 1852.
3. H. Lin, B. D. Storey, M. H. Oddy, C. H. Chen, and J. G. Santiago, Instability of Electrokinetic Microchannel Flows with Conductivity gradients, *Phys. Fluids*, vol. 16, pp. 1922–1935, 2004.
4. B. D. Storey, Direct Numerical Simulation of Electrohydrodynamic Flow Instabilities in Microchannels, *Physica D*, vol. 211, pp. 151–167, 2005.
5. G. Y. Tang, C. Yang, C. J. Chai, and H. Q. Gong, Modeling of Electroosmotic Flow and Capillary Electrophoresis with the Joule Heating Effect: The Nernst–Planck Equation versus the Boltzmann Distribution, *Langmuir*, vol. 19, pp. 10975–10984, 2003.
6. K. Horiuchi and P. Dutta, Joule Heating Effects in Electroosmotically Driven microchannel Flows, *Int. J. Heat Mass Transfer*, vol. 47, pp. 3085–3095, 2004.
7. G. Y. Tang, C. Yang, C. J. Chai, and H. Q. Gong, Joule Heating Effect on Electroosmotic Flow and Mass Species Transport in a Microcapillary, *Int. J. Heat Mass Transfer*, vol. 47, pp. 215–227, 2004.
8. G. Y. Tang, D. Yan, C. Yang, H. Q. Gong, C. J. Chai, and Y. C. Lam, Assessment of Joule Heating and Its Effects on Electroosmotic Flow and Electrophoresis Transport of Solutes in Microfluidic Channels, *Electrophoresis*, vol. 27, pp. 628–639, 2006.
9. R. F. Probstein, *Physicochemical Hydrodynamics: An Introduction,* 2nd ed., Wiley, New York, 1994.
10. J. H. Masliyah, *Electrokinetic Transport Phenomena*, Alberta Oil Sands Technology and Research Authority, Edmonton, Alberta, Canada, 1994.
11. R. Weast, M. J. Astle, and W. H. Beyer (eds.), *CRC Handbook of Chemistry and Physics*, CRC Press, Boca Raton, FL, 1986.
12. R. J. Hunter, *Zeta Potential in Colloid Science Principles and Applications*, Academic Press, New York, 1981.
13. D. W. Peaceman and H. H. Rachford, The Numerical Solution of Parabolic and Elliptic Differential Equations, *J. Soc. Ind. Appl. Math.*, vol. 3, pp. 28–41, 1955.
14. T. W. H. Sheu, S. K. Wang, and R. K. Lin, An Implicit Scheme for Solving the Convection-Diffusion-Reaction Equation in Two Dimensions, *J. Comput. Phys.*, vol. 164, pp. 123–142, 2000.
15. S. V. Patankar, *Numerical Heat Transfer and Fluid Flow*, Hemisphere, New York, 1980.
16. T. W. H. Sheu and R. K. Lin, An Incompressible Navier-Stokes Model Implemented on Nonstaggered Grids, *Numer. Heat Transfer B*, vol. 44, pp. 277–294, 2003.
17. T. W. H. Sheu and P. H. Chiu, A Divergence-Free-Condition Compensated Method for Incompressible Navier-Stokes Equations, *Comput. Meth. Appl. Mech. Eng.*, vol. 196, pp. 4479–4494, 2007.
18. P. Dutta and A. Breskok, Analytical Solution of Combined Electroosmotic/Pressure Driven Flows in Two-Dimensional Straight Channels: Finite Debye Layer Effects, *Anal. Chem.*, vol. 73, pp. 1979–1986, 2001.
19. D. Burgreen and F. R. Nakache, Electrokinetic Flow in Ultrafine Capillary Sites, *J. Phys. Chem.*, vol. 68, pp. 1084–1091, 1964.

Downloaded by [China Science & Technology University] at 02:33 26 February 2014